Biosensors and Bioelectronics 129 (2019) 155–163

Contents lists available at ScienceDirect

Biosensors and Bioelectronics

journal homepage: www.elsevier.com/locate/bios

An integrated microfluidic system with field-effect-transistor sensor arrays for detecting multiple cardiovascular biomarkers from clinical samples☆

Anirban Sinha[a], Tse-Yu Tai[a], Kuang-Hsien Li[c], Priya Gopinathan[a], Yi-Da Chung[b], Indu Sarangadharan[a], Hsi-Pin Ma[c], Po-Chiun Huang[c], Shu-Chu Shiesh[d], Yu-Lin Wang[a,b,*], Gwo-Bin Lee[a,b,e,**]

[a] Institute of NanoEngineering and Microsystems, National Tsing Hua University, Hsinchu, Taiwan
[b] Department of Power Mechanical Engineering, National Tsing Hua University, Hsinchu, Taiwan
[c] Department of Electrical Engineering, National Tsing Hua University, Hsinchu, Taiwan
[d] Department of Medical Laboratory Science and Biotechnology, National Cheng Kung University, Tainan, Taiwan
[e] Institute of Biomedical Engineering, National Tsing Hua University, Hsinchu, Taiwan

ARTICLE INFO

Keywords:
Aptamers
Biomarkers
Cardiovascular diseases
Field-effect transistors
Microfluidics

ABSTRACT

Certain blood-borne biomarkers offer a potent methodology for understanding the risk of cardiovascular diseases (CVDs) with clinicians generally advocating the use of multiple biomarkers for proper risk assessment of CVDs. Herein four such CVDs biomarkers- C-reactive protein (CRP), N-terminal pro b-type natriuretic peptide (NT-proBNP), cardiac troponin I (cTnI), and fibrinogen- were rapidly (5 min) analyzed from clinical samples (~ 4 μL) on an integrated microfluidic platform equipped with 1) immobilized highly specific aptamer probes and 2) field-effect transistor (FET)-based sensor arrays. The calibration curve from the FET sensor arrays showed good agreement in the physiological concentration ranges for CRP (0.1–50 mg/L), NT-proBNP (50–10,000 pg/mL), cTnI (1–10,000 pg/mL), and fibrinogen (0.1–5 mg/mL). The developed prototype of this fully automated portable device requires minimal reagent and sample inputs and consequently shows great promise for next-generation point-of-care devices assaying multiple CVDs biomarkers in clinical samples.

1. Introduction

Cardiovascular diseases (CVDs) are among the leading causes of death worldwide accounting for about 31% of all mortality (World Health Organization, 2016) and can lead to other disabling conditions (Celermajer et al., 2012). Although clinicians depend on a variety of tools to identify patients at the risk of CVDs (Mozaffarian et al., 2016; Vasan, 2006), current diagnostic protocols have their limitations. Assessing the risk of developing cardiovascular disease is an important aspect in clinical decision making for future prognostics and therapeutic strategy, and the use of serological biomarkers may improve this (Vasan, 2006), as the individuals displaying high concentrations of some well-validated CVD protein biomarkers are associated with higher risks of hemostasis, inflammation, and abnormal lipid metabolism (Skalny et al., 2017).

Numerous protein biomarkers, namely, fibrinogen (Stang and Mitchell, 2013), apolipoprotein B, cardiac troponin I (cTnI) (Sharma et al., 2004), N-terminal propeptide of B-type natriuretic peptide (NT-proBNP) (Panagopoulou et al., 2013), and C-reactive protein (CRP) (Pepys and Hirschfield, 2003) have been commonly used for CVD risk assessment, and clinicians generally advocate the quantification of multiple biomarkers (Thompson and Craig, 2011). For instance patients

Abbreviations: AlGaN/GaN, aluminum-gallium nitride/gallium nitride; CRP, C-reactive protein; CVDs, cardiovascular diseases; EDL, electrical double layer; ELISA, enzyme-linked immunosorbent assay; EMVs, electromagnetic valves; EDTA, Ethylenediaminetetraacetic acid; FET, field-effect transistor; HEMT, high electron mobility transistor; LCD, Liquid crystal display; LOD, Limit of detection; NT-proBNP, N-terminal pro b-type natriuretic peptide; PBS, phosphate buffer saline; PDMS, polydimethylsiloxane; PMMA, poly(methyl methacrylate); SELEX, Systematic evolution of ligands by exponential enrichment; SPR, surface plasmon resonance; TCEP, tris (2-carboxyethyl) phosphine hydrochloride; TE buffer, Tris-EDTA buffer; cTnI, human cardiac troponin I; ssDNA, single-stranded DNA

☆ Preliminary results found within this work were presented at the 31st IEEE International Conference on Micro Electro Mechanical Systems (MEMS 2018) held in Belfast, North Ireland between January 21 and 25 of 2018.

* Corresponding author at: Institute of NanoEngineering and Microsystems, National Tsing-Hua University, Hsinchu 30013, Taiwan.
** Corresponding author at: Department of Power Mechanical Engineering, National Tsing-Hua University, Hsinchu 30013, Taiwan.
E-mail addresses: ylwang@mx.nthu.edu.tw (Y.-L. Wang), gwobin@pme.nthu.edu.tw (G.-B. Lee).

https://doi.org/10.1016/j.bios.2019.01.001
Received 30 November 2018; Accepted 3 January 2019
Available online 04 January 2019
0956-5663/

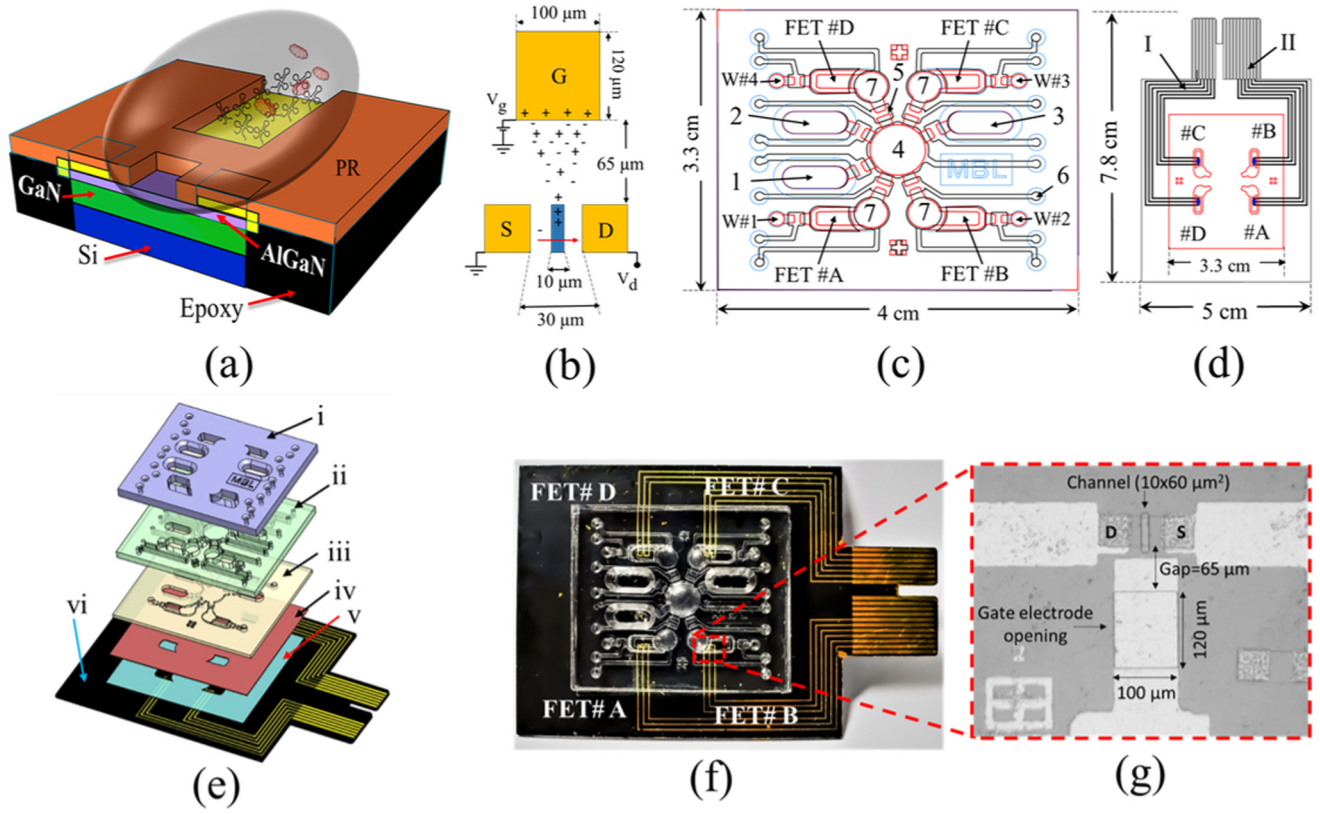

Fig. 1. High electron mobility transistor (HEMT)-microfluidic chip design: (a) HEMT sensor featuring different structural layers (PR = photoresist). In (b), the source (S), drain (D), and gate (G) of the FET sensor have been labeled. (c) The microfluidic chip consisted of several microfluidic devices and three reservoirs for storing purified proteins/serum/plasma (#1), washing buffer solution (#2), elution buffer (#3). A (normally-closed) micropump (#4), waste collection chambers (W#1, 2, 3, and 4), micromixer (#7), air inlet (#6), and four field-effect transistor (FET)/detection chambers (FET# A, B, C, and D [for aptamers specific to each of the four protein biomarkers]). (d) The microfluidic chip's detection chamber featuring the positions of the FET sensor arrays. The metal lines (#I) represent the connections between the FETs and the PCI (peripheral component interconnect) connector lines (#II). (e) An exposed view showing the different layers of the chip: top reagent reservoir (#i), pneumatic control layer (#ii), liquid flow channel layer (#iii), thin PDMS layer (#iv), double-sided tape (#v), and FET-embedded epoxy substrate (#vi). (f) A photograph of the integrated chip featuring a magnified view (g) of the FET (electric double layer (EDL)-gated FET) sensor.

with CRP concentrations of 1–3 mg/L are considered to be at moderate risk (Shrivastava et al., 2015), NT-proBNP concentrations above 300 pg/mL are high risk individuals (Toda et al., 2010), cTnI concentrations > 0.5 ng/mL may be lethal (Kim et al., 2010) and variation in the concentrations of fibrinogen (Ndrepepa et al., 2013) above or below 1.5–3 g/L may predict serious risk of CVDs.

Several detection techniques have been employed for the detection of the aforementioned protein biomarkers [CRP (Fakanya and Tothill, 2014; Tsai et al., 2007; Zhang et al., 2015), NT-proBNP (Bay et al., 2003; Song et al., 2017), cTnI (Sarangadharan et al., 2018; Yang et al., 2017), fibrinogen (Poon et al., 2012; Schlimp et al., 2015)]. In fact, there are several commercially available kits are in the market [CRP: CRP human ELISA kit (Thermo-Fisher Scientific, USA), NT-proBNP: Aviva Systems Biology, USA, cTnI: Eurolyser Diagnostica GmbH, Austria, fibrinogen: Arigo Biolaboratories (Taiwan)].

Unfortunately, the aforementioned commercial CVDs protein biomarker assays are expensive, time-consuming, prone to antibody-based high batch-to-batch variation (O'Sullivan, 2002) and plagued by antibody cross-reactivity issues (Panagopoulou et al., 2013; Sharma et al., 2004). In the quest for better affinity reagents, nucleic acid aptamers have shown great promise (Nafee et al., 2017). Aptamers are single-stranded DNA (ssDNA) or RNA with high affinity and specificity (Dupont et al., 2015). Due to non-dependence on animal hosts, their synthesis is relatively cheap and reproducible; moreover, they are characterized by better thermal stability (even at high humidity levels) and can be denatured reversibly (Keefe et al., 2010; Lakhin et al., 2013), their adaptability and modular nature are among their top attributes in terms of making a case for superior affinity reagents (Jayasena, 1999).

Recently, field-effect transistor (FET)-based biosensors have been recognized as fast, reliable, compact, power-efficient, and extremely sensitive (De Moraes and Kubota, 2016; Huang et al., 2013; Nayeli et al., 2015). For instance, aluminum-gallium nitride/gallium nitride (AlGaN/GaN) based HEMT type FET sensors have been broadly utilized for gas, chemical, and biological applications (Cheng et al., 2006; Kang et al., 2007; Pearton et al., 2004). However, conventional FET-based sensors featuring affinity reagents as probes face an intrinsic Debye length issue due to severe charge screening effects in solutions with high ionic strengths, such as blood or serum (Chu et al., 2017). Since dilution of the sample may cause structural changes in the proteins (Formaneck et al., 2006; Tsumoto et al., 2007), a modified system where the channel conductivity was modulated by an electrical double layer (EDL) formed in the test solution (i.e., between the device active area and the gate) was developed to overcome such charge screening issues (Chu et al., 2017).

In order to overcome the complexity of fluid handling, microfluidic technologies have emerged as a promising approach for an array of biomedical applications (Duncombe et al., 2015; Gravesen et al., 1993). Though such point-of-care (POC) devices have been explored in numerous fields (Chin et al., 2012), namely infectious disease detection, neurology, oncology, and ophthalmology, there is a notable lack of cardiology-based POC devices. As there is consequently a need for a portable POC device capable of detecting and measuring concentrations of key CVD biomarkers, we hereby report an integrated microfluidic

chip equipped with sensitive FET sensor arrays and aptamers as capture probes for detection of four CVD protein biomarkers (CRP, NT-proBNP, cTnI, and fibrinogen) from untreated clinical samples. Furthermore, we designed a portable system that could automate the entire detection process (including microfluidic flow control and FET signal measurements) without the need for human intervention.

2. Materials and methods

2.1. Microfluidic FET biosensor

The integrated platform comprised of FET sensor arrays embedded on an epoxy substrate and a microfluidic chip for execution of the detection process. The design of the AlGaN/GaN-based EDL-gated HEMT sensor (Chu et al., 2017) has been schematically illustrated in Fig. 1a–b. The five layered microfluidic chip was fabricated (Supplemental Fig. S1) in polydimethylsiloxane (PDMS, Sylgard 184A/B, Dow Corning, USA) and was equipped with four detection chambers, (abbreviated as A, B, C, and D; used for CRP, NT-proBNP, cTnI, and fibrinogen, respectively as shown in Fig. 1c–d and several micro devices for smooth and efficient functioning. The layered structure of the assembly could be found in Fig. 1e. More details regarding the chip and details process of the characterization of the device can be found in Supplemental methods M1 and M2 respectively.

2.2. Reagents and materials

The aptamers used in this study have been reported earlier (Huang et al., 2010; Sinha et al., 2018). Aptamers for CRP, NT-proBNP, cTnI, and fibrinogen were synthesized (Medclub Scientific, Taiwan) with 5′ thiol-modification at a stock concentration 50 μM and stored at 4 °C in Tris-EDTA (TE) buffer until further use. Human clinical samples were obtained for research purposes only from National Cheng Kung University Hospital (NCKUH) after approval by the ethics review committee of Taiwan (IRB No. B-ER-104-116). Proteins, washing buffer and other detailed list of the reagents and chemicals used herein has been provided in Supplemental methods M3.

2.3. Aptamer functionalized sensor preparation

Building the aptamer functionalized FET sensor included three processes: cleaning the surface of FET sensor, reduction of disulfide bonds formed in the thiol labeled aptamer, and aptamer immobilization through self-assembled monolayer. The surface of the sensor (gold, opened gate region) was cleaned via ultraviolet (UV)-ozone (40 W, 10 min, PSD PRO-UV4 234546012512, Novascan, USA) treatment. A working aptamer concentration of 5 μM was prepared by individually mixing the aptamer stock with freshly prepared Tris(2-carboxyethyl) phosphine hydrochloride (TCEP, 10 mM) to a final volume of 5 μL (for each sensor). It was then placed at room temperature for 1 h to ensure the reduction of any disulfide bonds formed in the aptamer followed by heating at 95 °C for 5 min and rapidly cooling in order to regenerate ssDNA featuring their unique 3D structures (Smestad and James Maher, 2013). The aptamer-TCEP mixture was dispensed into the detection chambers on the microfluidic chip and allowed to immobilize on the gold surface (Fig. 2a-1 and a-2) for 20 h. The integrated device was kept in a sealed, humidified chamber at 25 °C until further use (Kao et al., 2017).

2.4. Optimization of analytical conditions

All signals from the FETs were recorded with a semiconductor analyzer (B1500A/B1530 Agilent, USA). A DC bias of 2 V was applied as the drain voltage and a short duration (100 μs on-time) pulse of 0.5 V was applied to the separated gate electrode as the gate voltage. When test solution was placed on the sensor and as the gate pulse is turned on, the potential drops in the solution thereby changing the channel conductivity. The top view image (Fig. 1b) depicts the sensing area which is composed of the openings on the gate electrode (100 × 120 μm^2) and the FET active area or the channel (10 × 60 μm^2), which are spaced apart at a distance of 65 μm. The sample solution placed on the sensor covers the two open areas, simulating a liquid capacitor, with two conductive plates (the FET channel and gate electrode) sandwiching a dielectric medium (test solution). The separated gate FET structure which shows that changes to the solution capacitance will result in changes in the potential drop across the dielectric, leading to changes in drain current response (Chu et al., 2017). The solution capacitance can vary under different states: once the ionic strength of the test medium is varied, the change in surface property due to functionalization of the gate electrode, and the modification of the electrostatic interaction at the gate electrode EDL via receptor-ligand binding.

Prior to testing any protein biomarkers or clinical samples, the amount of immobilized aptamers on the bare gold surface of the FET gate electrodes was quantified as per our previous studies, with consideration of immobilization time (Kao et al., 2017), aptamer concentration (Kao et al., 2017), and opened gate electrode surface area (Chu et al., 2017). The device reading was recorded before and after the aptamer immobilization process, and similar quantities of aptamers were immobilized on the gold surface (Supplemental Fig. S2). FETs with similar electrical characteristics were chosen and aptamers for four different biomarkers were immobilized at the same time on respective FETs. Unbound aptamers from each detection chamber were removed by three repetitive washing steps (15 μL of washing buffer), followed by 1) micro-mixing (operated at a gauge pressure of − 39 kPa at 2 Hz for 30 s) and 2) waste collection. The FET reading was then recorded to determine surface immobilization conditions and to generate a baseline to be used in the experiments outlined below. Total charge defined in this work does not refer to the physical charges accumulated on the sensor surface. Instead, it refers to the integration of the output drain current (Supplemental Fig. S3a–b) over the time of gate pulse application and indexing total charge moderates the noises and leads to a better isolation of each signal (Chu et al., 2017).

2.5. Analytical performance of the microfluidic aptamer-FET sensor

After aptamer immobilization was confirmed (verified with change of electrical signal Fig. S2, S3a), each of the four target protein biomarkers were diluted to a series of physiological and risk concentrations in 1× phosphate buffer saline (PBS) containing bovine serum albumin (BSA; 4% [w/v] final concentration) (Chu et al., 2017). Each protein concentration (4 μL) was transported to the designated detection chamber and allowed to incubate for 5 min. The FET signal reading was then recorded to estimate the amount of protein bound to the aptamers. The samples were then discarded through the waste collection chamber. Elution buffer from the elution buffer reservoir was then transported to the detection chamber and allowed to mix (operated at a gauge pressure of − 39 kPa at 5 Hz) with the bound samples on the FET surface for 10 min. The rationale behind the use of elution buffer being complete elution or removal of any proteins still bound to the aptamer on the FET surface prior to the testing of next protein concentration. Three repetitive washing steps were conducted to completely remove any contaminants from the detection chamber (15 μL of washing buffer, at − 39 kPa at 5 Hz for 60 s), and the FET signal was recorded after the elution step and compared to the baseline signal (Supplemental Fig. S3). The schematic illustration of the whole process on FET and fluidic transport on the microfluidic chip has been detailed in Figs. 2(I) and 2(II) respectively. To demonstrate the feasibility of the capture probe, serially diluted protein concentrations were also analyzed without immobilizing the aptamer and the data was shown in Supplemental Fig. S4.

For clinical samples from CVDs patients, concentrations of the target proteins were measured by NCKUH. In order to evaluate the reliability

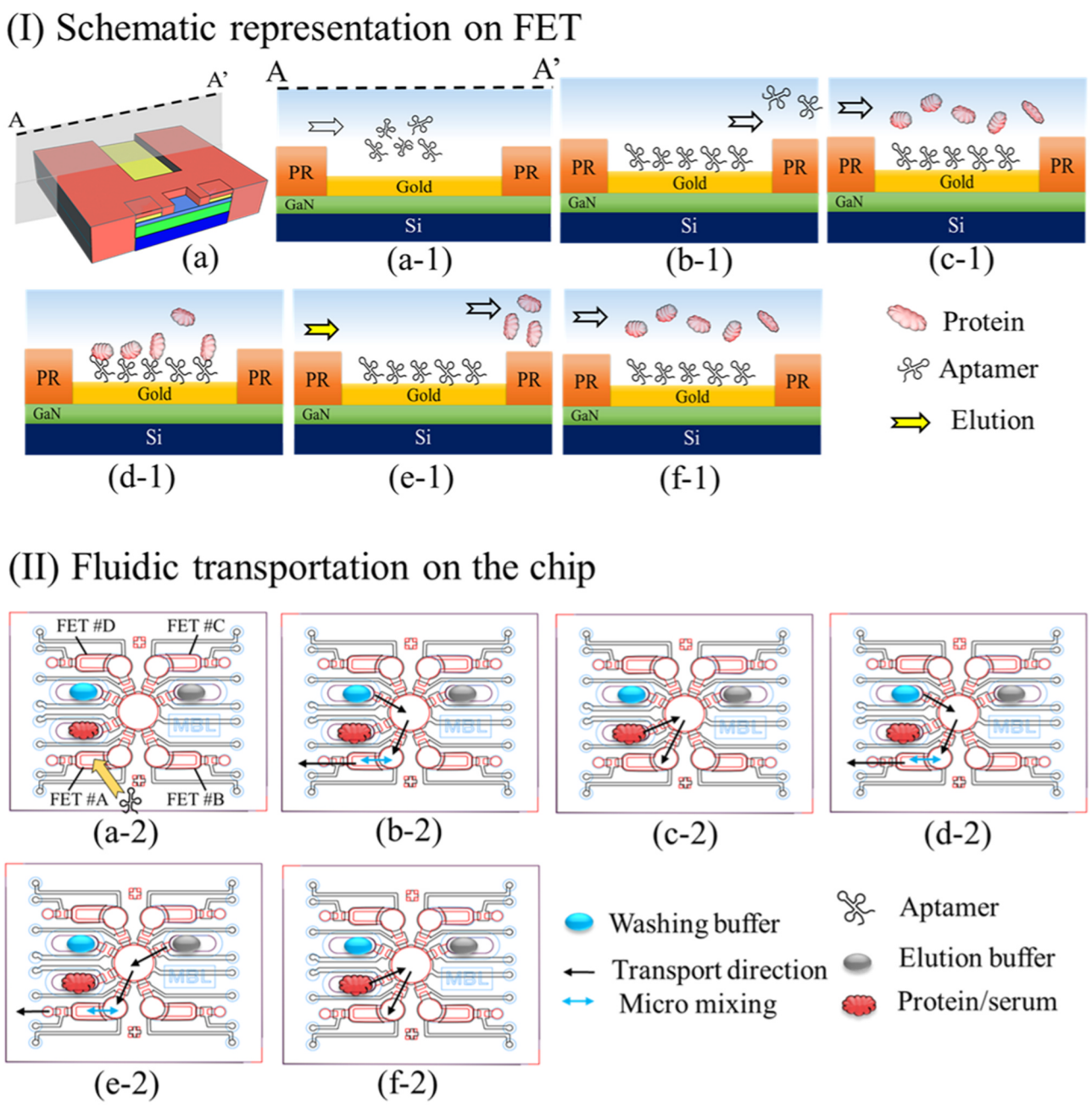

Fig. 2. Schematic representation of the protein biomarker detection process on (I) FET. For demonstration purposes, the FET-A chamber has been displayed in the figure, though similar processes were carried out in the other three chambers. (a) A lateral view of the HEMT sensor, in which the dotted lines encapsulate the area presented in the remainder of the figure. The detection process included (a-1) surface-immobilization of aptamers, (b-1) washing away of unbound aptamers, (c-1) addition of protein analytes, (d-1) capture of analytes by surface-immobilized aptamers on the FET surface, (e-1) elution, and (f-1) re-addition of analytes for further tests. FET measurements were made at step (b-1) to confirm surface immobilization of aptamers, step (d-1) to identify protein capture by the aptamers, and step (e-1) to confirm the elution success. (II) Fluidic transport on the microfluidic chip (a-2), Aptamers dissolved in TE (Tris-EDTA) buffer with TCEP was added to FET-A's open inlet and was immobilized over the course of 20 h. (b-2) Washing buffer was transported from a washing buffer chamber to wash away unbound aptamers. (c-2) Purified target proteins or patient serum/plasma was transported to FET-A and incubated for 5 min. (d-2, e-2) the sample was removed from the waste chamber and elution buffer was transported into FET-A, it was allowed to mix in the detection chamber for 10 min to remove any bound protein on the FET surface. (f-2) elution buffer was discarded and the detection chamber was washed using washing buffer thrice.

and application potential of the proposed FET biosensor, a spike-and-recovery experiment to assess any difference in the assay response was also conducted. Samples were prepared by spiking different concentrations of pure CRP, NT-proBNP, Troponin I and fibrinogen proteins into the patient serum samples in order to calculate the recovery rates.

2.6. Design of the portable control system

We developed a portable setup for pneumatic control of the chip and reading FET signals to detect the FET current gain (analogous to total charge) on the microfluidic platform. As the above-mentioned studies had been performed on a semiconductor analyzer, a custom-

made portable control system was specially created to run the pneumatically controlled microfluidic chip and read the FET signals in a manner that required minimal human intervention. The dual-compartment system (one for the pneumatic supply and another for electronic control) was constituted. The detailed components of this was described in a block diagram shown in Supplemental Fig. S5 and detailed part of the construction and components were detailed in Supplementary method M4.

3. Results and discussion

3.1. Optimization of the micro-devices on the chip

The microfluidic chip (3.3 cm × 4.0 cm) was optimized at several stages based upon our previous experiences (Kao et al., 2017). The following features of the chip were improved (data not shown): the thickness of the actuation membrane (200 μm), the width of the air supply channel, and the dimensions of the pneumatic (1100 μm height × 500 μm width) and liquid flow channel (200 μm height) layers. Regarding the former, a 200-μm-thick micro-membrane provided optimal membrane deflection and flexibility such that it could be used multiple times without tearing. The fluid transport was regulated by EMVs programmed to generate a local suction force from the compressed air inside the liquid flow channel layer (achieved by actuating the membrane from the pneumatic control channel). Fluids were mixed within the chip by a newly designed micromixer that represented a combination of an open-type chamber (detection chamber) and a connected, closed-type micropump (Supplemental Fig. S6). It is to be noted here that the conditions of operation of the entire experimental process was based on the above characterization. The four detection chambers of the chip contained EDL-gated HEMT sensor arrays, and all detection-related processes (i.e., capturing of target analytes followed by elution and washing) took place here. The washing process (i.e., removal of liquid from these chambers) was a critical step in minimizing false negative results. It was difficult to collect all liquid in the rectangular open chamber, since the fluids in close proximity to the waste collection outlet often escaped from the chamber, leaving some dead volume on the opposite side of the open-chamber. After several tests, a grooved micro-channel along the circumference of the detection chamber was fabricated (Supplemental Fig. S7). That worked as a capillary tube (100 μm × 400 μm) and had allowed the vacuum force to permeate evenly along the circumference of the detection/FET chamber.

Though packaging of a PDMS chip onto a different substrate has been attempted before (Kao et al., 2017), the packaging process was complicated and not reliable for large-scale production due to its large device-to-device variations and difficulty in packaging multiple sensors. Direct application of a double-sided tape onto the liquid layer for packaging reduces its performance due to the chances of leakage (air/liquid) through different movable parts of the microdevices (micromixers, normally-closed microvalves etc.). Solving the above issue, a thin PDMS layer was used to seal (PDMS-PDMS) the surrounding liquid channel layer (PDMS-PDMS). This kind of sealing provided uninterrupted liquid flow without compromising its packaging demands. Any sticky material (glue) could replace the double-sided tape used for bonding the PDMS layer with the epoxy substrate and this packaging process could be easily commercialized for mass production (Fig. 1e).

3.2. Characterization of the mixing and pumping devices on the microfluidic chip

The relationship between the liquid pumping rate of the micropump at different gauge pressures (− 13.3, − 26.6, − 39.9, − 53.3, − 59.2, − 66.6, and − 73.32 kPa) was tested (Fig. 3), and the maximum pumping rate was 2.85 μL/s at an operational gauge pressure of - 66.6 kPa at a driving frequency of 1 Hz. The maximum pumping rate was restricted at higher gauge pressures by the release time of the compressed air via PDMS membrane (Huang et al., 2012) actuation. This might explain why there was a decline in the pumping rate when the gauge pressure was increased from − 66.6 to − 73.32 kPa. Importantly, the micropump could deliver as little as ~ 4 μL in one complete cycle. It should also be stated here that the washing step executed with a micromixer with 20 μL of liquid (1 min, 3 times) was comparable to a benchtop washing protocol with 200–300 μL of the liquid. It was hypothesized that, due to a higher rate of diffusion during a micromixing process (described later), the overall device performance has increased.

The open-type chamber was combined with the closed-type micropump to facilitate the micromixer, and different operational gauge pressures (− 10 to − 50 kPa) were investigated to determine the level required for optimal mixing. A gauge pressure of − 39.9 kPa along with a 12-kPa compressive gauge pressure actuated the micromixer in a manner that prevented overflow. The performance of the newly designed micromixer was then evaluated at different operating frequencies (0.5, 1.0, 2.0, 4.0, and 5 Hz) with an applied positive gauge pressure of 12 kPa and a negative gauge pressure of − 39.9 kPa (Fig. 3b), and the time required for complete mixing decreased at higher driving frequencies. At a driving frequency of 0.5 Hz, ~ 5 s were required for complete mixing while an operating frequency of 5 Hz generated a similar mixing efficiency in 1 s (Fig. 3). Better mixing efficiencies inside the detection chamber ensured a uniform distribution of analytes and a significant reduction in reagent volume and mixing time .

3.3. Analytical performance of the microfluidic aptamer based FET biosensor

In order to evaluate the analytical performance of the aptamer-FET biosensor, different concentrations of proteins were measured under their optimal physiological and risk concentrations. Log-linear scatterplots of total charge (a proxy for aptamer-target protein concentration) against serial dilutions of physiologically relevant concentrations (in 1× PBS containing 4% BSA) of CRP (Fig. 4a), NT-proBNP (Fig. 4b), cTnI (Fig. 4c), and fibrinogen (Fig. 4d) are depicted. Total charge was increased with increasing input concentrations of the CRP protein while the total charge decreased with increasing protein concentrations for the other three protein biomarkers. Meanwhile, the limit of detection (LOD) of the aptamer based FET biosensor was calculated according to LOD = $3.3S_b/m$ (where S_b is the standard deviation of the blank and m is the slope of linear regression equation). Limit of quantification values have also been calculated as per the equation LOQ = $10S_b/m$ and have been detailed for each protein in Table S1. The LOD values for CRP, NT-proBNP, cTnI and fibrinogen were found to be 0.14 mg/L, 0.832 pg/mL, 0.394 pg/mL and 20.2 mg/dL respectively (Supplemental method M5 and Supplemental Table S1). Based upon the LOD values of 1 ng/mL and 1.95 pg/mL with commercially available assay kits for cTnI and NT-proBNP respectively, it is concluded that the sensitivity of the developed microfluidic FET biosensor is superior. For CRP and fibrinogen, LOD values from our biosensor seems to be comparable to the assay kits currently available in the market.

3.4. Detection of proteins from clinical samples and recovery rate measurements

The developed system was used to quantify CVDs biomarker concentrations from markedly more complex patient clinical samples (Fig. 4e–h), and total charge was plotted (log-linear) against various protein concentrations for CRP (Fig. 4e; 3.0, 3.1, 8.0, 18.5, 23.2, and 33.4 mg/L), NT-proBNP (Fig. 4f; 52.6, 507.6, 1105, 1854, and 3085 pg/mL), cTnI (Fig. 4g; 45, 665, 728, 529, and 9089 pg/mL), and fibrinogen (Fig. 4h; 0.77, 1.65, 1.94, 1.97, 2.97, and 6.70 mg/mL), and an ascending trend was detected for the former protein only; descending trend were instead documented for the other three proteins as was also

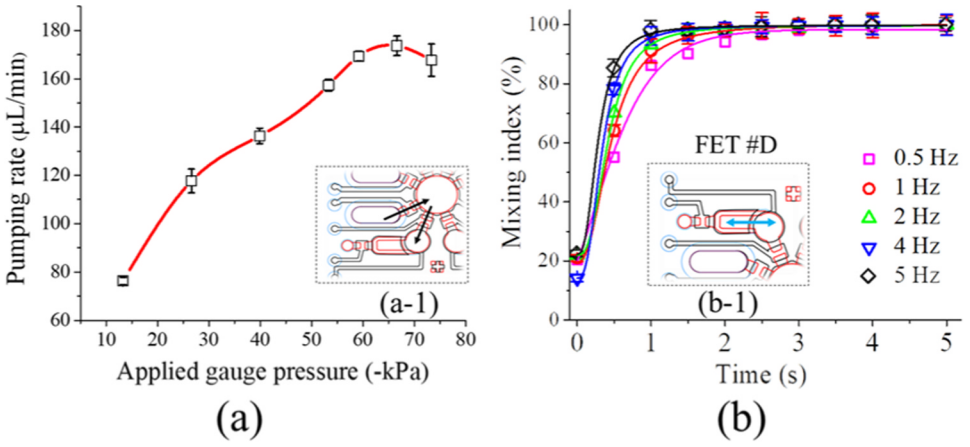

Fig. 3. Microfluidic device characterization and on-chip detection: (a) The pumping rate of the micropump as a function of gauge pressure. A partial view of the chip has been presented in an inset (a-1) to demonstrate the flow direction (as black arrows). (b) The efficiency of micro-mixing was tested in the detection chamber by applying a gauge pressure of − 39.9 kPa as the micro-membrane was fluctuated at various frequencies (0.5, 1,2, 4, or 5 Hz).

the case for the purified target proteins (Fig. 4). This may be attributed to the fact that electrostatic gating effects of the negatively charged aptamer on the channel surfaces may result in increase or decrease in carrier concentration and aptamers undergo significant conformational changes upon binding with ligands, which might affect the conductance modulation of underlying channel layers (Kim et al., 2015), Collectively, these data show that the developed system could detect physiologically meaningful concentrations of four CVDs biomarkers within a short period of time (5 min) in an automatic fashion than for previously published methods for the detection of CRP (Fakanya and Tothill, 2014), NT-proBNP (Regmi et al., 2017; Song et al., 2017), cTnI (Han et al., 2016; Sarangadharan et al., 2018), and fibrinogen (Lee et al., 2015; Regmi et al., 2017).

Owing to the complexity of the serum samples which may contain components that affect assay response to the analytes differently than the standard diluents, recovery rates were analyzed. The recovery rates for the four proteins has been detailed in Supplemental Table S2. The recovery rates were in an acceptable range of 90–103% for CRP, 91–93% for NT-proBNP, 96–107% for Troponin I and 92–98% for fibrinogen, indicating the good accuracy of the biosensor in the complex samples. This may also be attributed to the 'beyond Debye length' testing capability of the FET sensor at high salt concentrations. As a result, no dilution of the biological sample is required.

The stability of the as developed microfluidic-FET biosensor was evaluated under consecutive cyclic testing and elution experiments with the protein biomarker, CRP. A concentration of 1 mg/L in 1 × PBS (pH 7.4) was used for the above experiments. As shown in Supplementary Fig. S3(c), the accumulated total charges did not show

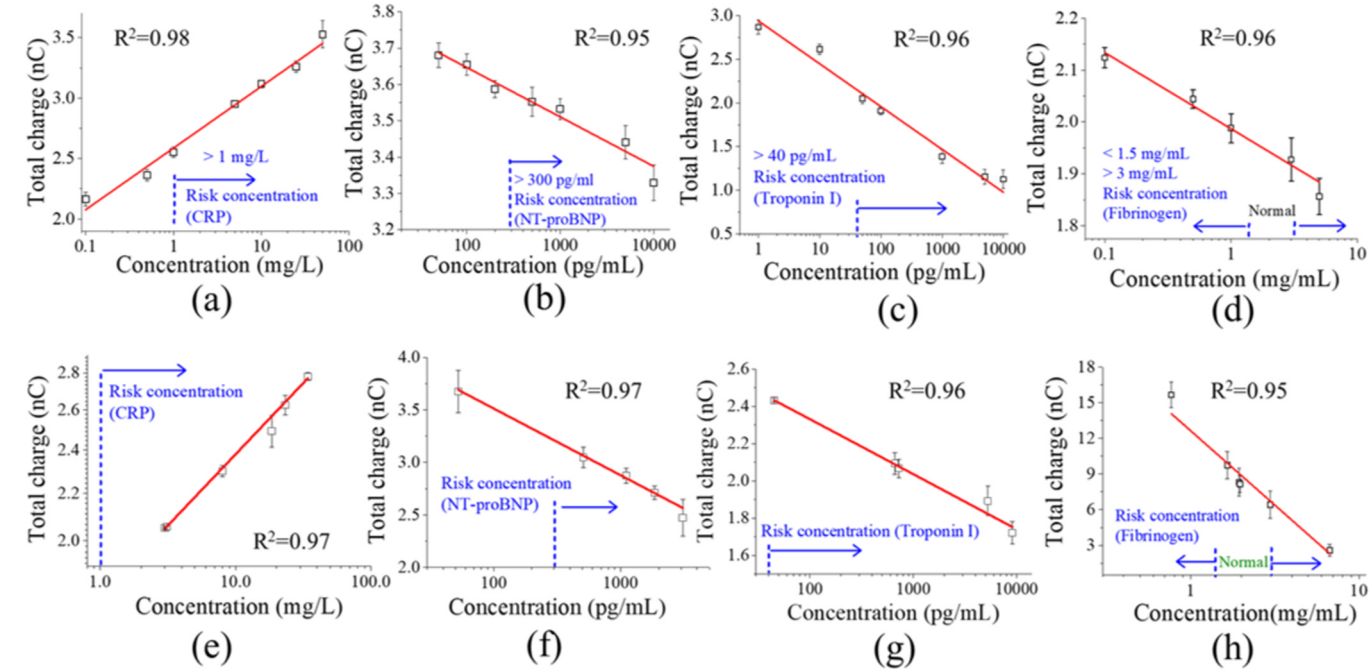

Fig. 4. Total charge as a function of purified protein and serum/plasma sample input. Total charge (determined by FET) against concentrations of purified protein (with 4% BSA) for four cardiovascular diseases (CVDs) biomarkers. The best-fit line slopes showed an ascending trend for (a) CRP and descending trend for (b) NT-proBNP, (c) cTnI, and (d) fibrinogen. The subsequent risk threshold concentration has also been marked. Error bars represent (n = 3). A plot of total charge (nC; determined using human clinical samples as the input biological material. The best-fit lines showed an increasing trend for (e) CRP and decreasing trends for (f) NT-proBNP, (g) cTnI, and (h) fibrinogen with increasing protein concentrations. The associated risk concentration has also been shown for each marker. Error bars represent standard deviations (n = 3).

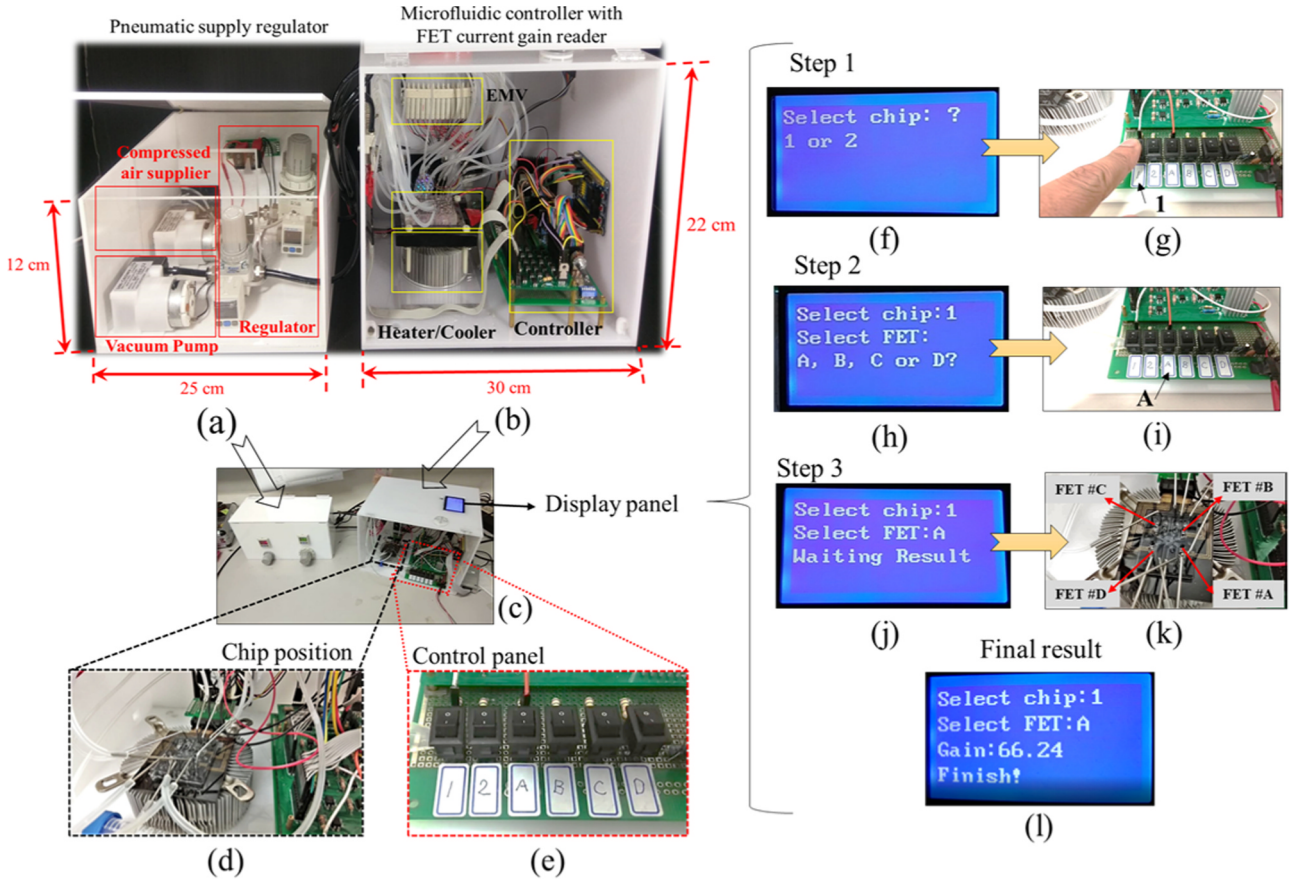

Fig. 5. The portable control system: the portable system consisted of two compartments; the left compartment (a) supplied the air that regulated the actuation amplitude of the microfluidic micro-membrane. (b) The right compartment contained the electromagnetic valve (EMV) control module, the temperature control module, and the FET signal reader. (c) The minimized photograph of the complete setup for prospective point-of-care applications. (d) The aerial magnified view of FET equipped microfluidic chip and 9e) control panel. Demonstration of the working process of the portable system as demonstrated with LCD panel instructions in three steps utilizing one of the four detection chambers (FET A). The steps include (f–g) selection of the microfluidic chip (h-i) selection of FET detection units (FET# A, B, C, D) (j-k) the controller initiated the fluidic transport on the FET integrated microfluidic chip (l) and display panel showed the corresponding gain of FET. The gain value was comparable to a pre-calibrated chip and corresponding concentrations could be interpreted.

any obvious changes and the related standard deviation (RSD) was only 3.3%, which suggested the proposed system has good stability.

3.5. Portable control system

The fabricated device was tested by a home-made portable control system (Fig. 5) that was assembled such that it could be used in a POC setup without any manual process or human interference. The prototype consisted of two separate cases; the first (25 × 12 × 15 cm) as shown in Fig. 5a was designed for pneumatic control of the chip, and the second case (55 × 25 × 22 cm) as shown in Fig. 5b featured the main electronic control unit. A minimized view of the control system has been shown in Fig. 5c, d and e depict the chip position and control panel respectively. The result of the concentration was displayed on the LCD monitor. All the processes of the microfluidic control were programmed into the embedded system such that the fluidic control and detection was automated. The display panel as shown displays the steps of operation which was depicted in Fig. 5f–g (selection of chip number out of two), Fig. 5h-I (selection of FET chamber for initiating detection process), Fig. 5j–k (microfluidic flow processes required for chosen FET chamber) and finally Fig. 5l showed the current gain measured by FET reader. The concentration-dependent current gain from a calibrated chip could represent an unknown analyte concentration.

4. Conclusions and future potential of the developed system

This study has demonstrated an integrated microfluidic chip featuring EDL gated HEMT-FET sensor arrays that could detect (in mostly applicable physiological risk concentration range) four major CVDs protein biomarkers (with the aid of a portable control device) from human clinical samples (~ 4 μL) in only five minutes. The developed system utilized four highly specific aptamers as probes, which were able to bind protein biomarkers from complex serum/plasma samples, are likely to be more stable than their protein-based counterparts. The low-power, FET-based system provides accurate results rapidly and could be scaled up for mass production. The portable, user-friendly, POC control system combined a highly sensitive FET sensor that worked beyond the Debye length to detect analytes isolated on-chip. To the best of our knowledge, this is the only reported setup capable of detecting four CVDs protein biomarkers from a single clinical sample in an area of only 4.0 × 3.3 cm. Given the high demand for POC systems (Chin et al., 2012), this type of multiple-analyte detector could play an important role, either alongside, or in place of, more traditional, commercial systems (Table 1: De Moraes and Kubota, 2016) for CVDs diagnostics. Furthermore, it could be readily modified to feature immobilized aptamer probes specific to biomarkers diagnostic of other life-threatening illnesses.

Table 1
Comparison of a typical commercially available ELISA kit, a traditional FET sensor system (De Moraes and Kubota, 2016), and the system developed herein for profiling cardiovascular diseases (CVDs) biomarkers. POC = point-of-care.

Characteristic	Commercial kit	FET sensor	System developed herein
Overall properties	Antibody-based ELISA kit	Affinity (antibody)-based, poor sensitivity in physiological media	Affinity (aptamer)-based, EDL-gated, functions beyond Debye length
Response time	10–30 min	5–20 min, though highly variable	5 min
Labels	Labeling needed	Direct detection	Direct detection
Sample volume	mL range	System-dependent	~ 4 μL
Sensitivity	Low detection limit	Poor sensitivity in clinical specimen	Low detection limit in clinical sample
Work place/storage	Proper storage needed, hospital-based	System-dependent	Usable anywhere
Size	Small kit, portable	Variable	Large but portable
Cost	Very expensive	Cheap	Cheap
Automation	Bench top, manual	Manual (most cases)	Fully automated with microfluidics and portable controller
Sample treatment/process	Multiple steps, manual	Dilution needed	Direct detection
Temperature	Highly sensitive	Antibody-based systems are temperature sensitive	Stable at a wide range
POC capability	None	Mostly incapable	Capable
Multiplexing capacity	None (single analyte)	None (single analyte)	Capable of detecting multiple biomarkers (at least four)

Acknowledgments

The authors would like to thank the Ministry of Science and Technology (MOST) of Taiwan (MOST 106-2221-E-007-001 and MOST 107-2221-E-007-013-MY3 to GBL) for funding this work. Partial financial support from the Ministry of Education of Taiwan's Higher Education Sprout Project (Grant no. 107Q2713E1) is also greatly appreciated.

Declaration of interests

None.

Appendix A. Supplementary material

Supplementary data associated with this article can be found in the online version at doi:10.1016/j.bios.2019.01.001.

References

Bay, M., Kirk, V., Parner, J., Hassager, C., Nielsen, H., 2003. NT-proBNP: a new diagnostic screening tool to differentiate between patients with normal and reduced left ventricular systolic function. Heart.

Celermajer, D.S., Chow, C.K., Marijon, E., Anstey, N.M., Woo, K.S., 2012. Cardiovascular disease in the developing world. J. Am. Coll. Cardiol. 60, 1207–1216. https://doi.org/10.1016/j.jacc.2012.03.074.

Cheng, C.C., Tsai, Y.Y., Lin, K.W., Chen, H.I., Hsu, W.H., Hong, C.W., Liu, W.C., 2006. Characteristics of a Pd–oxide–$In_{0.49}Ga_{0.51}P$ high electron mobility transistor (HEMT)-based hydrogen sensor. Sens. Actuators B Chem. 113, 29–35. https://doi.org/10.1016/J.SNB.2005.02.019.

Chin, C.D., Linder, V., Sia, S.K., 2012. Commercialization of microfluidic point-of-care diagnostic devices. Lab Chip 12, 2118. https://doi.org/10.1039/c2lc21204h.

Chu, C.H., Sarangadharan, I., Regmi, A., Chen, Y.W., Hsu, C.P., Chang, W.H., Lee, G.Y., Chyi, J.I., Chen, C.C., Shiesh, S.C., Lee, G.B., Wang, Y.L., 2017. Beyond the Debye length in high ionic strength solution: direct protein detection with field-effect transistors (FETs) in human serum. Sci. Rep. 7, 5256. https://doi.org/10.1038/s41598-017-05426-6.

De Moraes, A., Kubota, L., 2016. Recent trends in field-effect transistors-based immunosensors. Chemosensors 4, 20. https://doi.org/10.3390/chemosensors4040020.

Duncombe, T.A., Tentori, A.M., Herr, A.E., 2015. Microfluidics: reframing biological enquiry. Nat. Rev. Mol. Cell Biol. 16, 554–567. https://doi.org/10.1038/nrm4041.

Dupont, D.M., Thuesen, C.K., Bøtkjær, K.A., Behrens, M.A., Dam, K., Sørensen, H.P., Pedersen, J.S., Ploug, M., Jensen, J.K., Andreasen, P.A., 2015. Protein-binding RNA aptamers affect molecular interactions distantly from their binding sites. PLoS One 10, 1–22. https://doi.org/10.1371/journal.pone.0119207.

Fakanya, W.M., Tothill, I.E., 2014. Detection of the inflammation biomarker C-reactive protein in serum samples: towards an optimal biosensor formula. Biosensors 4, 340–357. https://doi.org/10.3390/bios4040340.

Formaneck, M.S., Ma, L., Cui, Q., 2006. Effects of temperature and salt concentration on the structural stability of human lymphotactin: insights from molecular simulations. J. Am. Chem. Soc. 128, 9506–9517. https://doi.org/10.1021/ja061620o.

Gravesen, P., Branebjerg, J., Jensen, O.S., 1993. Microfluidics – a review. J. Micromech. Microeng. 3, 168–182. https://doi.org/10.1088/0960-1317/3/4/002.

Han, X., Li, S., Peng, Z., Othman, A.M., Leblanc, R., 2016. Recent development of cardiac troponin I setection. ACS Sens. 1, 106–114. https://doi.org/10.1021/acssensors.5b00318.

Huang, C.C., Lee, G.Y., Chyi, J.I., Cheng, H.T., Hsu, C.P., Hsu, Y.R., Hsu, C.H., Huang, Y.F., Sun, Y.C., Chen, C.C., Li, S.S., Andrew Yeh, J., Yao, D.J., Ren, F., Wang, Y.L., 2013. AlGaN/GaN high electron mobility transistors for protein–peptide binding affinity study. Biosens. Bioelectron. 41, 717–722. https://doi.org/10.1016/j.bios.2012.09.066.

Huang, C.J., Lin, H.I., Shiesh, S.C., Lee, G.B., 2012. An integrated microfluidic system for rapid screening of alpha-fetoprotein-specific aptamers. Biosens. Bioelectron. 35, 50–55. https://doi.org/10.1016/j.bios.2012.02.024.

Huang, C.J., Lin, H.I., Shiesh, S.C., Lee, G.B., 2010. Integrated microfluidic system for rapid screening of CRP aptamers utilizing systematic evolution of ligands by exponential enrichment (SELEX). Biosens. Bioelectron. 25, 1761–1766. https://doi.org/10.1016/j.bios.2009.12.029.

Jayasena, S.D., 1999. Aptamers: an emerging class of molecules that rival antibodies in diagnostics. Clin. Chem. 45, 1628–1650.

Kang, B.S., Wang, H.T., Lele, T.P., Tseng, Y., Ren, F., Pearton, S.J., Johnson, J.W., Rajagopal, P., Roberts, J.C., Piner, E.L., Linthicum, K.J., 2007. Prostate specific antigen detection using AlGaN/GaN high electron mobility transistors. Appl. Phys. Lett. 91, 112106. https://doi.org/10.1063/1.2772192.

Kao, W.C., Chen, Y.W., Chu, C.H., Chang, W.H., Shiesh, S.C., Wang, Y.L., Lee, G.B., 2017. Detection of C-reactive protein on an integrated microfluidic system by utilizing field-effect transistors and aptamers. Biomicrofluidics 11, 044105. https://doi.org/10.1063/1.4995257.

Keefe, A.D., Pai, S., Ellington, A., 2010. Aptamers as therapeutics. Nat. Rev. Drug Discov. 9, 537–550. https://doi.org/10.1038/nrd3141.

Kim, J., Rim, Y.S., Chen, H., Cao, H.H., Nakatsuka, N., Hinton, H.L., Zhao, C., Andrews, A.M., Yang, Y., Weiss, P.S., 2015. Fabrication of high-performance ultrathin In_2O_3 film field-effect transistors and biosensors using chemical lift-off lithography. ACS Nano 9, 4572–4582. https://doi.org/10.1021/acsnano.5b01211.

Kim, W.J., Kim, B.K., Kim, A., Huh, C., Ah, C.S., Kim, K.-H., Hong, J., Park, S.H., Song, S., Song, J., Sung, G.Y., 2010. Response to cardiac markers in human serum analyzed by guided-mode resonance biosensor. Anal. Chem. 82, 9686–9693. https://doi.org/10.1021/ac101716p.

Lakhin, A.V., Tarantul, V.Z., Gening, L.V., 2013. Aptamers: problems, solutions and prospects. Acta Nat. 5, 34–43.

Lee, J., Dak, P., Lee, Y., Park, H., Choi, W., Alam, M.A., Kim, S., 2015. Two-dimensional layered MoS_2 biosensors enable highly sensitive detection of biomolecules. Sci. Rep. 4, 7352. https://doi.org/10.1038/srep07352.

Mozaffarian, D., Benjamin, E.J., Go, A.S., Arnett, D.K., Blaha, M.J., Cushman, M., Das, S.R., Ferranti, S., De, Després, J.P., Fullerton, H.J., Howard, V.J., Huffman, M.D., Isasi, C.R., Jiménez, M.C., Judd, S.E., Kissela, B.M., Lichtman, J.H., Lisabeth, L.D., Liu, S., MacKey, R.H., Magid, D.J., McGuire, D.K., Mohler, E.R., Moy, C.S., Muntner, P., Mussolino, M.E., Nasir, K., Neumar, R.W., Nichol, G., Palaniappan, L., Pandey, D.K., Reeves, M.J., Rodriguez, C.J., Rosamond, W., Sorlie, P.D., Stein, J., Towfighi, A., Turan, T.N., Virani, S.S., Woo, D., Yeh, R.W., Turner, M.B., 2016. Heart disease and stroke statistics-2016 update a report from the American Heart Association. Circulation 133, e38–e48. https://doi.org/10.1161/CIR.0000000000000350.

Nafee, N., Taetz, S., Schneider, M., Schaefer, U.F., Lehr, C.M., Nimjee, S.M., White, R.R., Becker, R.C., Sullenger, B.A., 2017. Aptamers as therapeutics. Annu. Rev. Pharmacol. Toxicol. 57, 61–79. https://doi.org/10.1146/annurev-pharmtox-010716-104558.

Nayeli, E., Stefan, S.U., Volker, C., Oliver, A., 2015. Sips adsorption model for DNA sensing with AlGaN/GaN high electron mobility transistors (IMRC2014-2B-O003). MRS Proc. 1763. https://doi.org/10.1557/opl.2015.131.

Ndrepepa, G., Braun, S., King, L., Fusaro, M., Keta, D., Cassese, S., Tada, T., Schömig, A., Kastrati, A., 2013. Relation of fibrinogen level with cardiovascular events in patients with coronary artery disease. Am. J. Cardiol. 111, 804–810. https://doi.org/10.1016/J.AMJCARD.2012.11.060.

O'Sullivan, C.K., 2002. Aptasensors – the future of biosensing? Anal. Bioanal. Chem. 372, 44–48. https://doi.org/10.1007/s00216-001-1189-3.

Panagopoulou, V., Deftereos, S., Kossyvakis, C., Raisakis, K., Giannopoulos, G., Bouras, G., Pyrgakis, V., Cleman, M.W., 2013. NTproBNP: an important biomarker in vardiac diseases. Curr. Top. Med. Chem. 13, 82–94. https://doi.org/10.2174/1568026611313020002.

Pearton, S.J., Kang, B.S., Kim, S., Ren, F., Gila, B.P., Abernathy, C.R., Lin, J., Chu, S.N.G., 2004. GaN-based diodes and transistors for chemical, gas, biological and pressure sensing. J. Phys. Condens. Matter 16, R961–R994. https://doi.org/10.1088/0953-8984/16/29/R02.

Pepys, M.B., Hirschfield, G.M., 2003. C-reactive protein: a critical update. J. Clin. Invest. 111, 1805–1812. https://doi.org/10.1172/JCI18921.

Poon, K.W.C., Lyng, F.M., Knief, P., Howe, O., Meade, A.D., Curtin, J.F., Byrne, H.J., Vaughan, J., 2012. Quantitative reagent-free detection of fibrinogen levels in human blood plasma using Raman spectroscopy. Analyst 137, 1807. https://doi.org/10.1039/c2an35042d.

Regmi, A., Sarangadharan, I., Chen, Y.W., Hsu, C.P., Lee, G.Y., Chyi, J.I., Shiesh, S.C., Lee, G.B., Wang, Y.L., 2017. Direct detection of fibrinogen in human plasma using electric-double-layer gated AlGaN/GaN high electron mobility transistors. Appl. Phys. Lett. 111, 082106. https://doi.org/10.1063/1.5000247.

Sarangadharan, I., Regmi, A., Chen, Y.W., Hsu, C.P., Chen, P., chi, Chang, W.H., Lee, G.Y., Chyi, J.I., Shiesh, S.C., Lee, G.B., Wang, Y.L., 2018. High sensitivity cardiac troponin I detection in physiological environment using AlGaN/GaN high electron mobility transistor (HEMT) biosensors. Biosens. Bioelectron. 100, 282–289. https://doi.org/10.1016/J.BIOS.2017.09.018.

Schlimp, C.J., Khadem, A., Klotz, A., Solomon, C., Hochleitner, G., Ponschab, M., Redl, H., Schöchl, H., 2015. Rapid measurement of fibrinogen concentration in whole blood using a steel ball coagulometer. J. Trauma Acute Care Surg. 78, 830–836. https://doi.org/10.1097/TA.0000000000000546.

Sharma, S., Jackson, P.G., Makan, J., 2004. Cardiac troponins. J. Clin. Pathol. 57, 1025–1026. https://doi.org/10.1136/jcp.2003.015420.

Shrivastava, A.K., Singh, H.V., Raizada, A., Singh, S.K., 2015. C-reactive protein, inflammation and coronary heart disease. Egypt. Heart J. 67, 89–97. https://doi.org/10.1016/J.EHJ.2014.11.005.

Sinha, A., Gopinathan, P., Chung, Y., Da, Lin, H.Y., Li, K.H., Ma, H.P., Huang, P.C., Shiesh, S.C., Lee, G.B., 2018. An integrated microfluidic platform to perform uninterrupted SELEX cycles to screen affinity reagents specific to cardiovascular biomarkers. Biosens. Bioelectron. 122, 104–112. https://doi.org/10.1016/j.bios.2018.09.040.

Skalny, A.V., Klimenko, L.L., Turna, A.A., Budanova, M.N., Baskakov, I.S., Savostina, M.S., Mazilina, A.N., Deyev, A.I., Skalnaya, M.G., Tinkov, A.A., 2017. Serum trace elements are associated with hemostasis, lipid spectrum and inflammatory markers in men suffering from acute ischemic stroke. Metab. Brain Dis. 32, 779–788. https://doi.org/10.1007/s11011-017-9967-6.

Smestad, J., James Maher, L., 2013. Ion-dependent conformational switching by a DNA aptamer that induces remyelination in a mouse model of multiple sclerosis. Nucleic Acids Res. 41, 1329–1342. https://doi.org/10.1093/nar/gks1093.

Song, K.S., Nimse, S.B., Sonawane, M.D., Warkad, S.D., Kim, T., 2017. Ultra-sensitive NT-proBNP quantification for early detection of risk factors leading to heart failure. Sensors 17, 2116. https://doi.org/10.3390/s17092116.

Stang, L.J., Mitchell, L.G., 2013. Fibrinogen. Methods Mol. Biol. 181–192. https://doi.org/10.1007/978-1-62703-339-8_14.

Thompson, P.L., Craig, I.H., 2011. Coronary Care Manual, Coronary Care Manual. Elsevier, Australia. https://doi.org/10.1016/B978-0-7295-3927-2.10007-7.

Toda, K., Sato, Y., Hara, T., Hijiya, K., Kaneko, R., Okada, T., Takatsu, Y., Fujiwara, H., Iwasaki, T., 2010. Correlates of NT-proBNP concentration in patients with essential hypertension in absence of congestive heart failure. J. Clin. Lab. Anal. 24, 12–16. https://doi.org/10.1002/jcla.20366.

Tsai, H.Y., Hsu, C.F., Chiu, I.W., Bor Fuh, C., 2007. Detection of C-reactive protein based on immunoassay using antibody-conjugated magnetic nanoparticles. Anal. Chem. 79, 8416–8419. https://doi.org/10.1021/ac071262n.

Tsumoto, K., Ejima, D., Senczuk, A.M., Kita, Y., Arakawa, T., 2007. Effects of salts on protein–surface interactions: applications for column chromatography. J. Pharm. Sci. 96, 1677–1690. https://doi.org/10.1002/jps.20821.

Vasan, R.S., 2006. Biomarkers of cardiovascular disease: molecular basis and practical considerations. Circulation 113, 2335–2362. https://doi.org/10.1161/CIRCULATIONAHA.104.482570.

World Health Organization, 2016. Hearts: Technical Package for Cardiovascular Disease Management in Primary Health Care. . 〈http://www.who.int/cardiovascular_diseases/publications/en/〉.

Yang, J., Carey, P., Ren, F., Wang, Y.L., Good, M.L., Jang, S., Mastro, M.A., Pearton, S.J., 2017. Rapid detection of cardiac troponin I using antibody-immobilized gate-pulsed AlGaN/GaN high electron mobility transistor structures. Appl. Phys. Lett. 111, 202104. https://doi.org/10.1063/1.5011151.

Zhang, P., Bao, Y., Draz, M.S., Lu, H., Liu, C., Han, H., 2015. Rapid and quantitative detection of C-reactive protein based on quantum dots and immunofiltration assay. Int. J. Nanomed. 10, 6161–6173. https://doi.org/10.2147/IJN.S89307.